Supporting information

Fe(III) protoporphyrin IX encapsulated in a zinc metal-organic framework shows dramatically enhanced peroxidatic activity

*Nicola A. Dare[a], Lee Brammer[b], Susan A. Bourne[a] and Timothy J. Egan[a,]**

[a] Department of Chemistry, University of Cape Town, Private Bag, Rondebosch 7701, South Africa; [b] Department of Chemistry, University of Sheffield, Brook Hill, Sheffield S3 7HF, United Kingdom; E-mail: Timothy.Egan@uct.ac.za

Table of contents

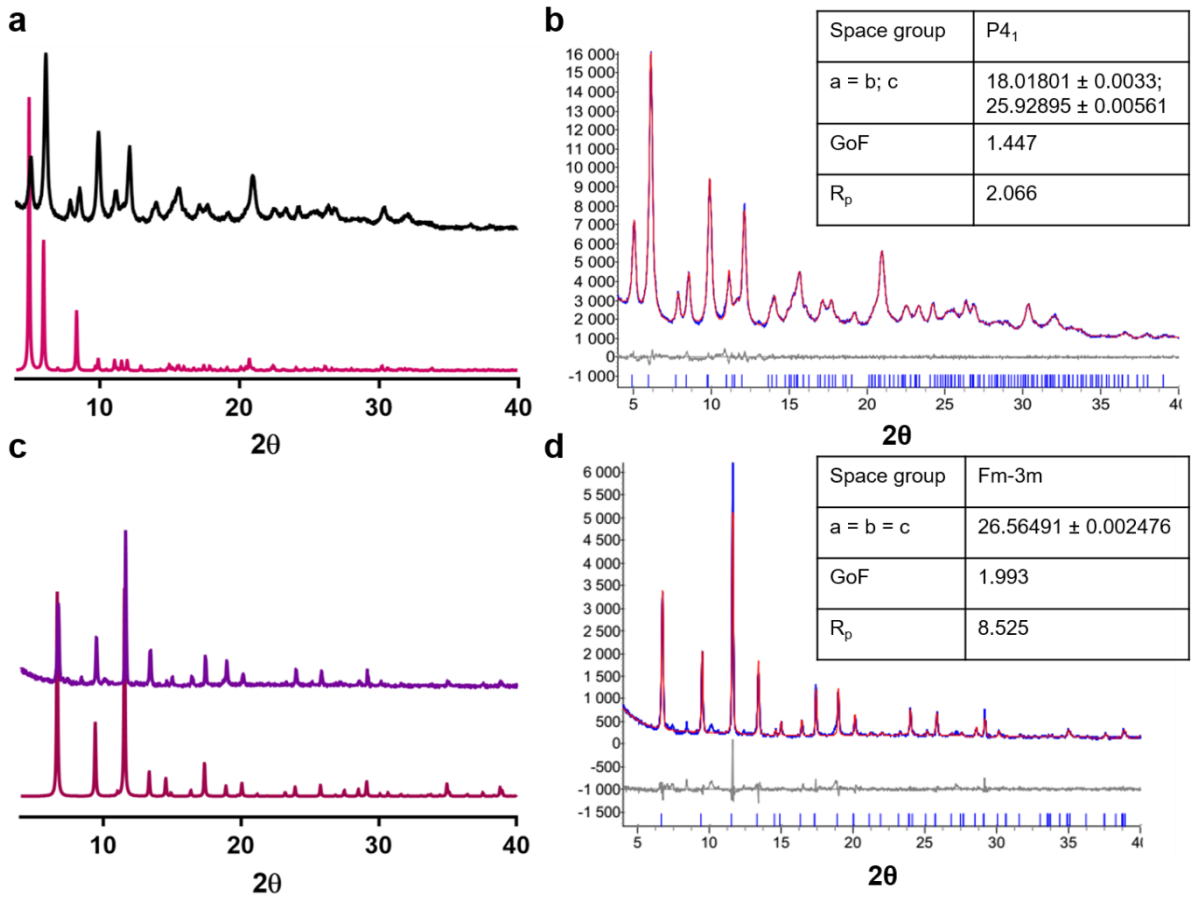

Figure S1: *(a) PXRD of* ***1*** *as synthesized (black) compared to calculated pattern (pink) of* ***1***[1]*; (b) Pawley fitting of* ***1*** *as synthesized. Experimental pattern (blue), calculated pattern (red), difference pattern (expt-calc) (grey). Unit cell dimensions and agreement indices are shown in the inset and are in good agreement with the unit cell of the calculated pattern; (c) PXRD of* ***2*** *as synthesized (purple) compared to calculated pattern (pink);*[2] *(d) Pawley fitting of* ***2*** *as synthesized. Experimental pattern (blue), calculated pattern (red), difference pattern (expt-calc) (grey). Unit cell dimensions and agreement indices are shown in the inset and are in good agreement with the unit cell of the calculated pattern. PXRD patterns were collected on a Bruker D8 Advance with Cu Kα radiation (λ = 1.54060 Å). The sample was ground and the pattern was collected over a 2θ range of 4 – 40° with a step size of 0.02° with 2 s exposure per step.*

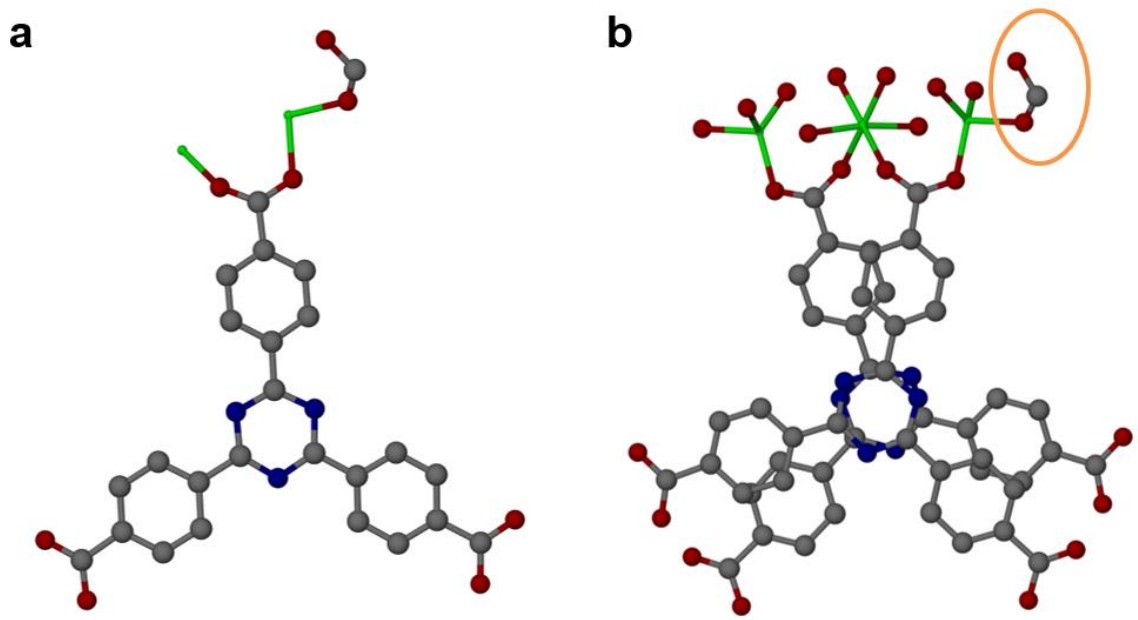

Figure S2: *Crystal structure of* ***1.*** *(a) Asymmetric unit of* ***1*** *with hydrogen atoms not shown for clarity; (b) Coordination environment of Zn ions in* ***1.*** *Bridging formate group is circled in orange. The structure of* ***1*** *is identical to the previously reported crystal structure of this framework.*[1]

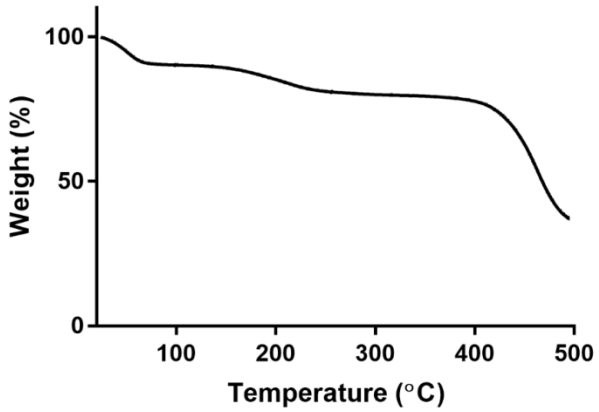

Figure S3: *TGA of* ***1*** *showing a 20.9 ± 1.1 % mass loss due to the presence of solvent molecules. Degradation of the framework begins at approximately 400 ℃.*

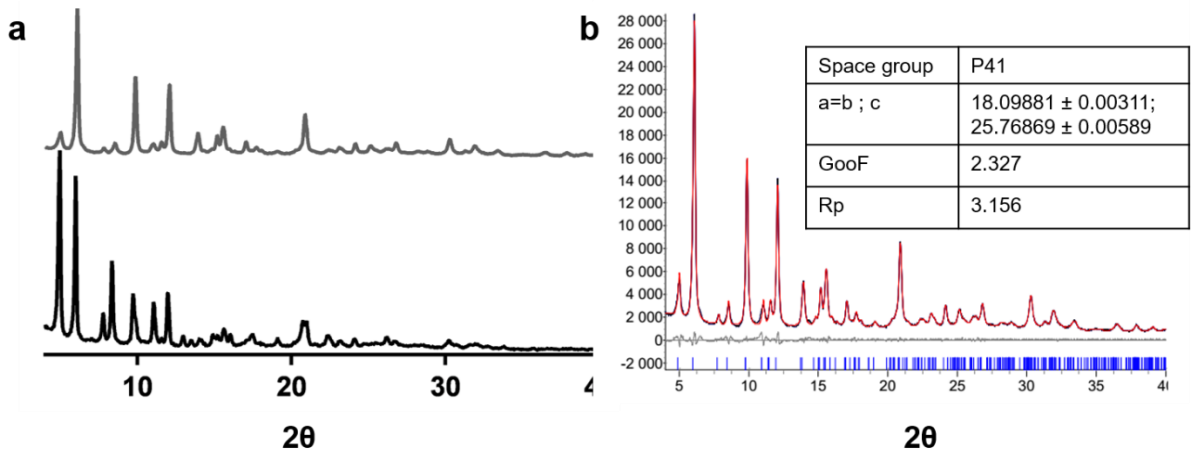

Figure S4*: (a) PXRD of* ***1*** *before (black) and after (gray) exposure to an aqueous solution; (b) Pawley fitting of* ***1*** *exposed to water for 12 h. Experimental pattern (blue), calculated pattern (red), difference pattern (expt-calc) (grey). Unit cell dimensions and agreement indices are shown in the inset and are in good agreement with the unit cell of the calculated pattern. PXRD patterns were collected on a Bruker D8 Advance with Cu Kα radiation (λ = 1.54060 Å). The sample was ground and the pattern was collected over a 2θ range of 4 – 40° with a step size of 0.02° with 2 s exposure per step.*

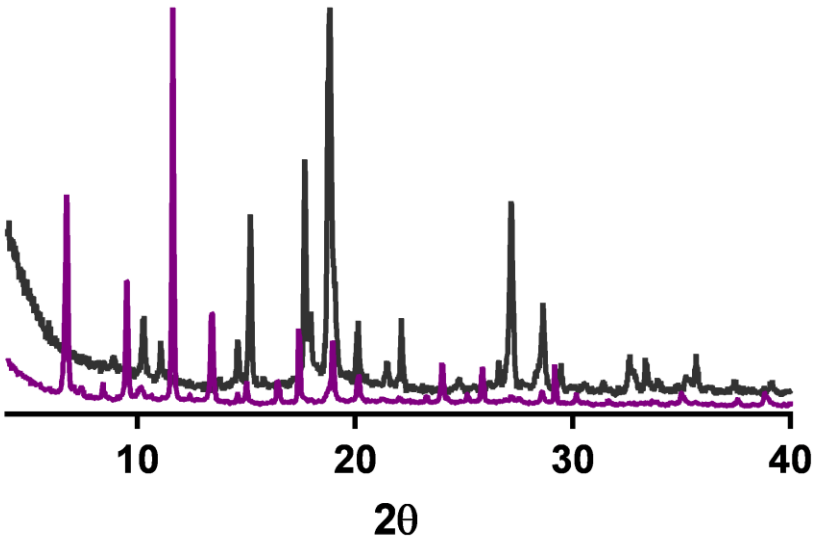

Figure S5*: PXRD of* ***2*** *before (purple) and after (black) exposure to an aqueous solution. PXRD patterns were collected on a Bruker D8 Advance with Cu Kα radiation (λ = 1.54060 Å). The sample was ground and the pattern was collected over a 2θ range of 4 – 40° with a step size of 0.02° and 2 s exposure per step.*

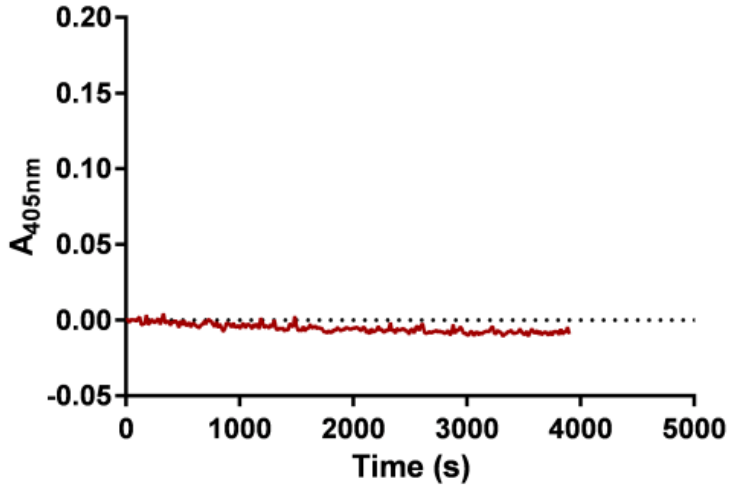

Figure S6*: No evidence of catalyst leaching – no increase in absorbance at 405 nm was observed from Fe(III)PPIX leached out of the catalyst. 1 mg of Fe(III)PPIX-**1** was placed in 2.5 mL of 0.01 M TRIS (pH 7.4) in a cuvette with constant stirring. The absorbance at the position of the Soret band (405 nm) was monitored over time. Any leaching of Fe(III)PPIX from Fe(III)PPIX-**1** would result in an increase in absorbance at 405 nm.*

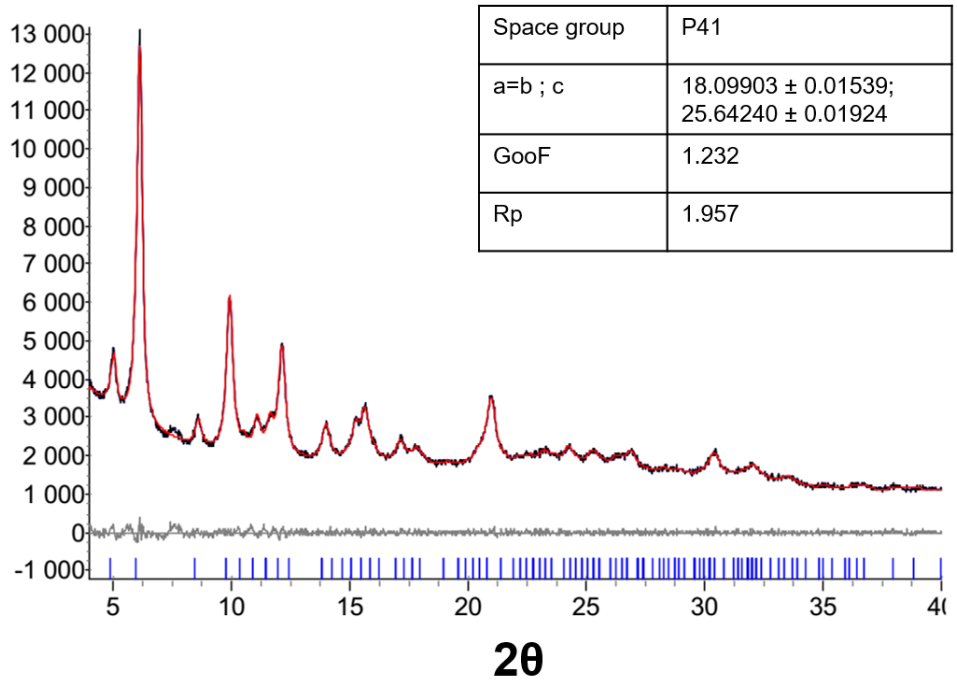

Figure S7: *Pawley fitting of Fe(III)PPIX-**1** confirming that there were minimal changes to the unit cell upon encapsulation of Fe(III)PPIX into **1** compared to the fitted unit cell of **1** (a = b = 18.09881; c = 25.76869) (Fig S1). Experimental pattern (blue), calculated pattern (red), difference pattern (expt-calc) (grey). Unit cell dimensions and agreement indices are shown in the inset. PXRD patterns were collected on a Bruker D8 Advance with Cu Kα radiation (λ = 1.54060 Å). The sample was ground and the pattern was collected over a 2θ range of 4 – 40° with a step size of 0.02° with 2 s exposure per step.*

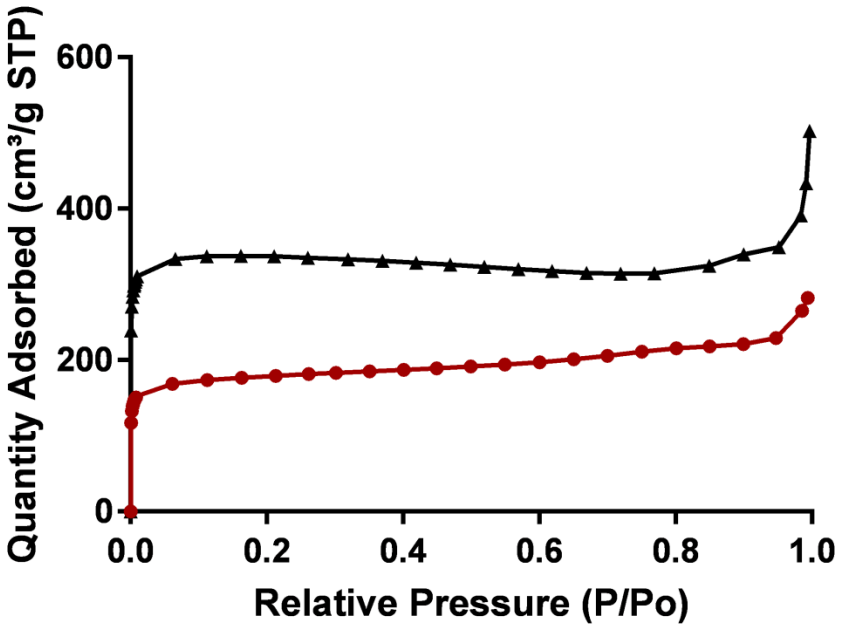

Figure S8: *N_2 sorption isotherms of **1** (black) and Fe(III)PPIX-**1** (red) at -196 °C.*

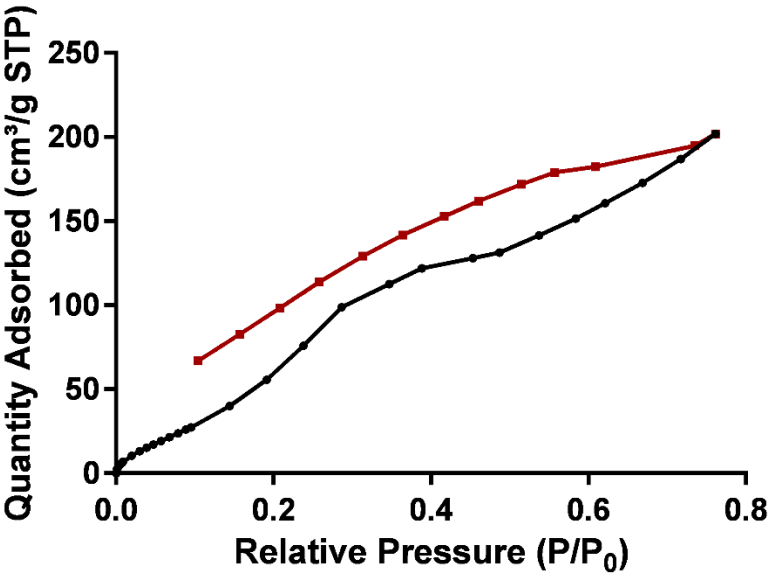

Figure S9: *Water sorption (black) and desorption (red) isotherms of Fe(III)PPIX-**1** at 25 °C.*

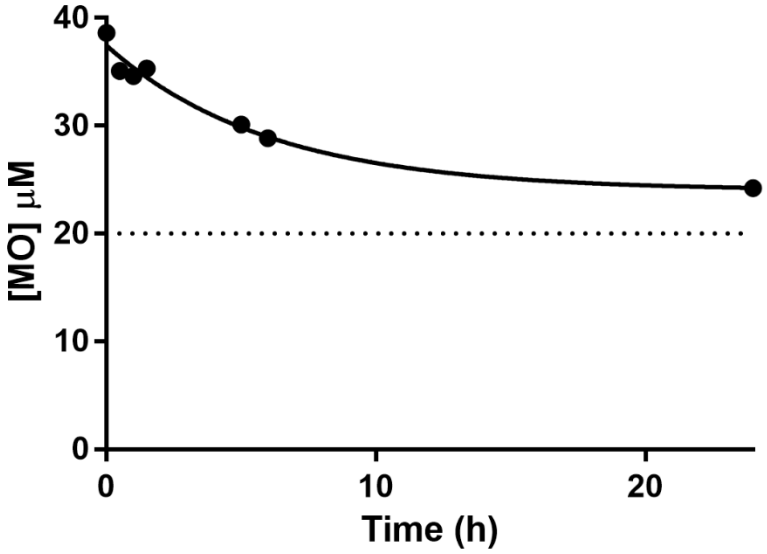

Figure S10: *Oxidation of MO by H_2O_2 in the presence of Fe(III)PPIX-**1**. In this experiment 2.82 mg of Fe(III)PPIX-**1** (0.50 µmol Fe(III)PPIX-**1**) was added to 4.75 mL of a 2 mM aqueous MO solution (0.01 M TRIS, pH 7.4). The reaction was initiated by adding 250 µL of 20 mM H_2O_2 (final concentration of 1 mM H_2O_2). The reaction was monitored by removing 100 µL aliquots of the reaction mixture at fixed time points. These aliquots were diluted in 2.5 ml 0.01 M TRIS buffer (pH 7.4) and the spectra were read on a Shimadzu UV-1800 spectrometer at 25.00 ± 0.02 °C. The decrease of the λ_{max} of MO at 465 nm was plotted against reaction time. Data were analyzed using the one-phase exponential function in GraphPad Prism.*[3] *The % conversion was calculated using the concentration of the limiting reagent, H_2O_2, that can oxidize a maximum of 1mM MO (of 2mM present in the reaction mixture). Dotted line indicates theoretical concentration of MO after 100 % oxidation by H_2O_2 catalyzed by Fe(III)PPIX-**1**.*

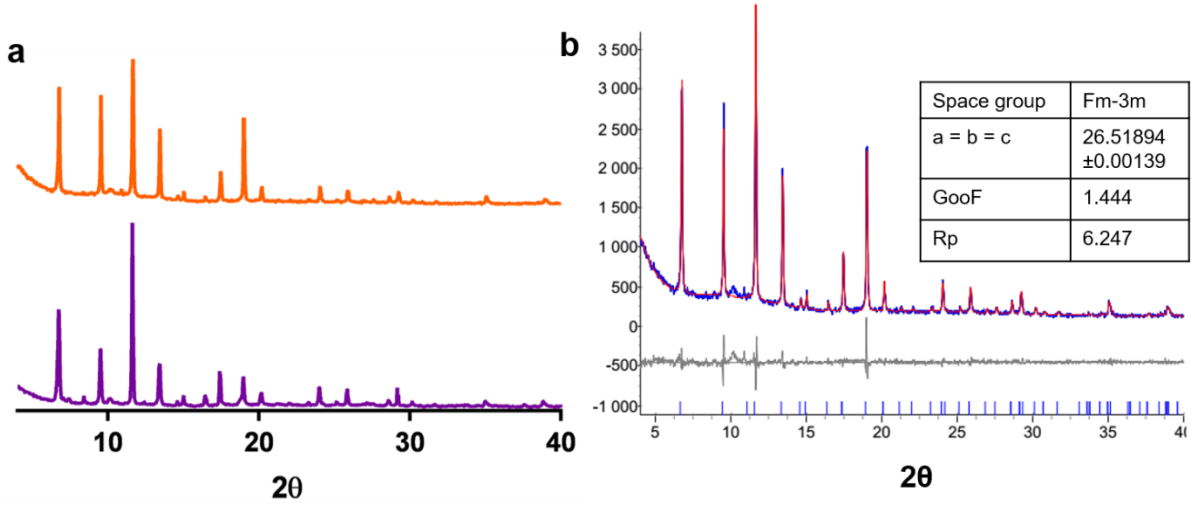

***Figure S11**: (a) PXRD of **2** (purple) compared to synthesized Fe(III)PPIX-**2** (orange); (b) Pawley fitting of Fe(III)PPIX-**2** as synthesized. Slight contamination is evident from the presence of small peaks at 6° and 9.5° resulting in a poor Pawley fit at these values of 2θ. Experimental pattern (blue), calculated pattern (red), difference pattern (expt-calc) (grey). Unit cell dimensions and agreement indices are shown in the inset and are in good agreement with the unit cell of **2**. PXRD patterns were collected on a Bruker D8 Advance with Cu Kα radiation (λ = 1.54060 Å). The sample was ground and the pattern was collected over a 2θ range of 4 – 40° with a step size of 0.02° with 2 s exposure per step.*

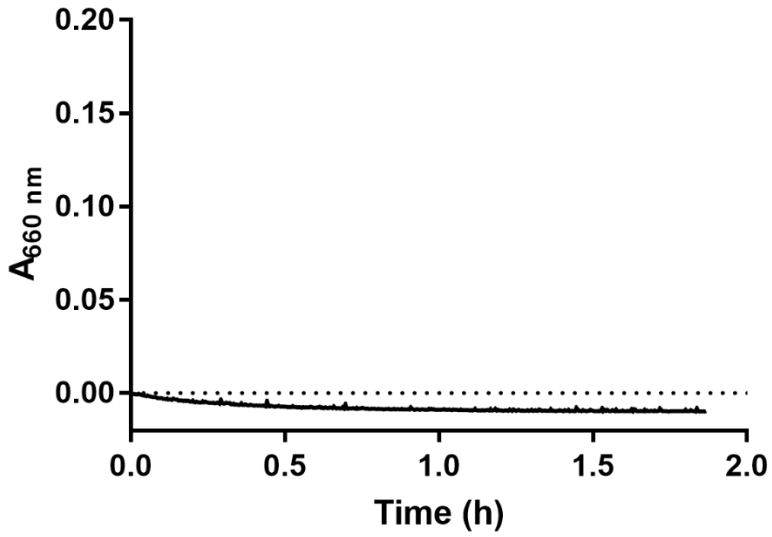

Figure S12*: Lack of oxidation of ABTS by* ***1****. No increase in absorbance at 660 nm corresponding to the formation of ABTS*$^{\bullet+}$ *is observed under standard reaction conditions (1 mg* ***1*** *added as a "catalyst").*

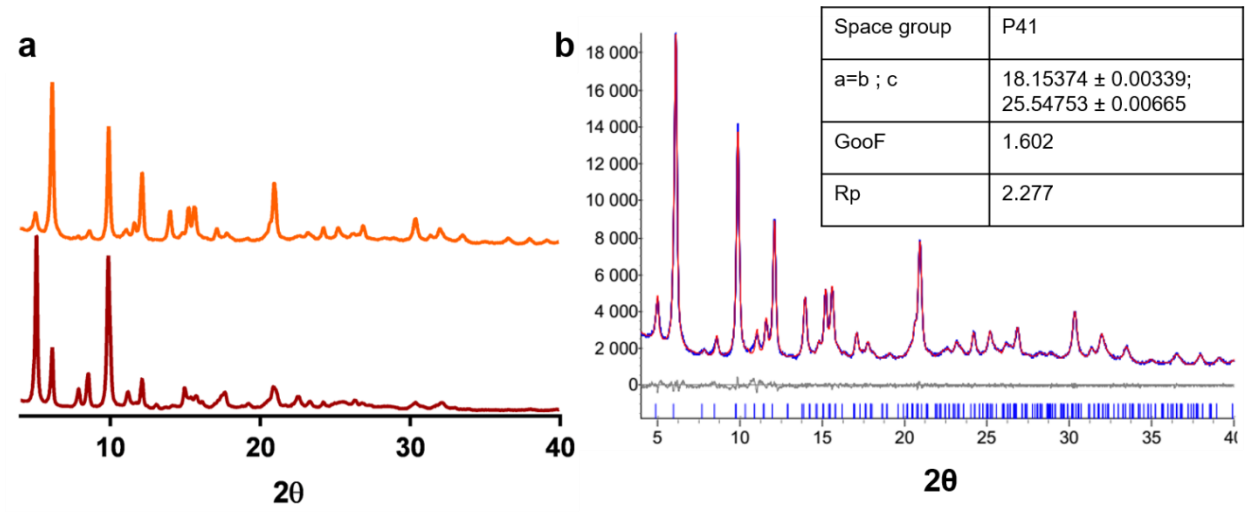

Figure S13*: (a) PXRD comparison of Fe(III)PPIX-**1** (red) and the same material after five successive cycles of ABTS oxidation (orange) showing minimal changes and that Fe(III)PPIX-**1** retained its structural integrity; (b) Pawley fitting of Fe(III)PPIX-**1** after five cycles of ABTS oxidation. Experimental pattern (blue), calculated pattern (red), difference pattern (expt-calc) (grey). Unit cell dimensions and agreement indices are shown in the inset and are in good agreement with the unit cell of Fe(III)PPIX-**1**.*

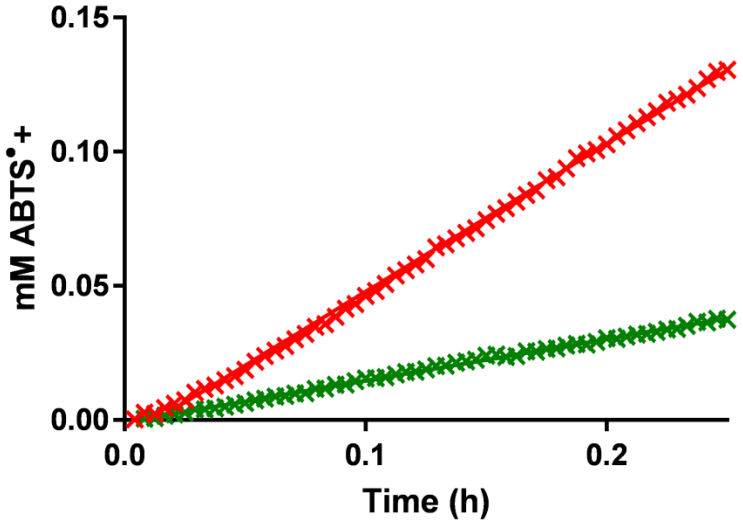

Figure S14: *Initial rates of oxidation of ABTS by H_2O_2 (green) and ^{t}BuOOH (red) catalyzed by Fe(III)PPIX-**1** in H_2O.*

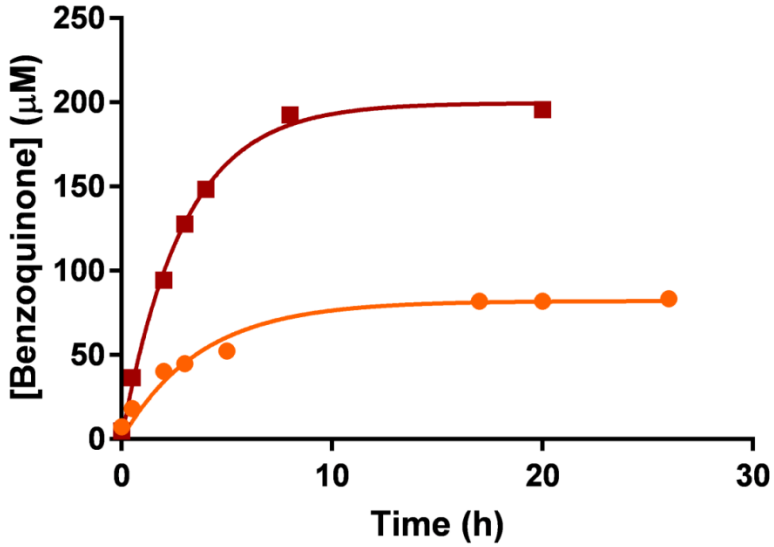

Figure S15: *Increase of product in catalytic oxidation of hydroquinone by ^{t}BuOOH in AcN catalysed by Fe(III)PPIX-**1** (red) and Fe(III)PPIX-**2** (orange), fitted with a non-linear regression model in Graph Pad Prism to determine the half-life of each reaction*

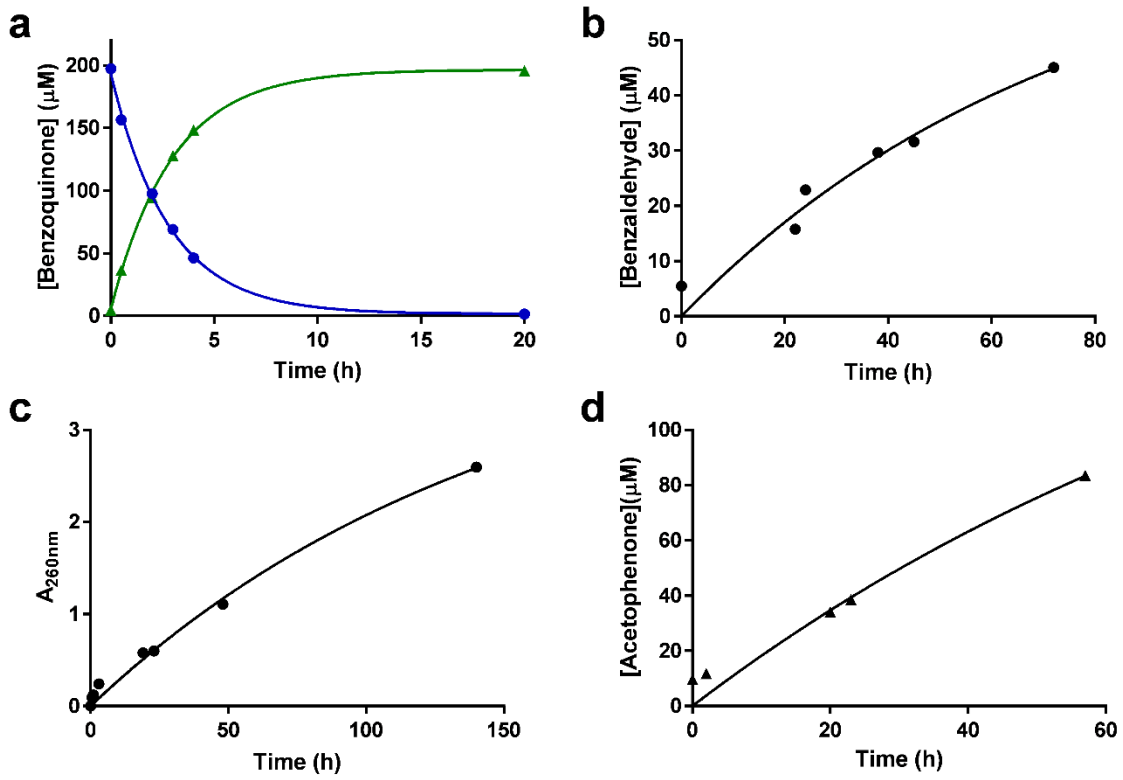

Figure S16*: Increase of product in catalytic oxidation of (a) benzoquinone (green) and decrease of hydroquinone (blue), increase in (b) benzyl alcohol, (c) thymol and (d) phenyl ethanol by* ^{t}*BuOOH in AcN catalysed by Fe(III)PPIX-**1**, fitted with a non-linear regression model in Graph Pad Prism to determine the half-life of each reaction.*

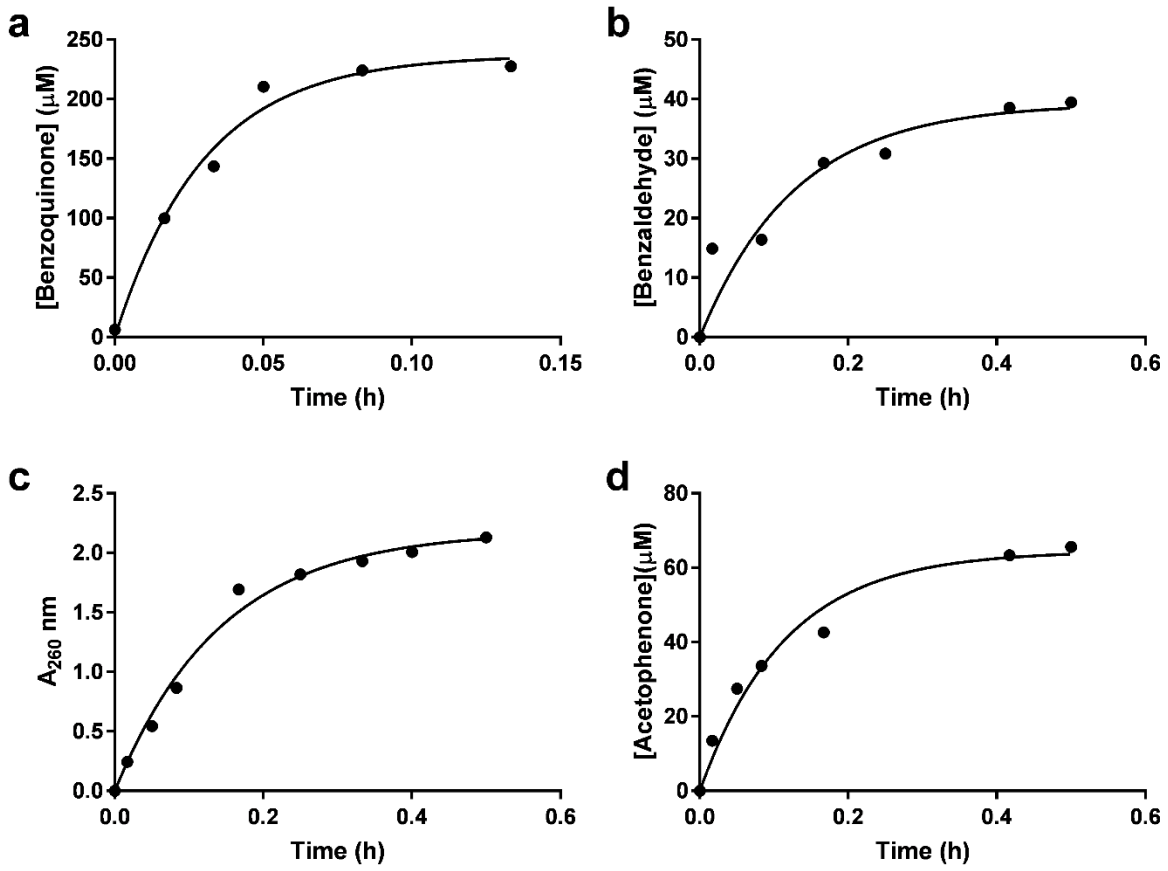

Figure S17*: Increase of product in catalytic oxidation of (a) hydroquinone, increase in (b) benzyl alcohol, (c) thymol and (d) phenyl ethanol by* ^{t}*BuOOH in AcN catalyzed by Fe(III)PPIX in solution, fitted with a non-linear regression model in Graph Pad Prism to determine the half-life of each reaction.*

Table S1: Conversion, half-lives and molar volumes of substrates oxidized by ^{t}BuOOH in the presence of Fe(III)PPIX in solution

Substrate	**Product**	**Catalyst loading**	**Conversion (Solution)[a]**	**Half-life (solution) (h)[b]**	**Molecular volume (Å^3)[c]**
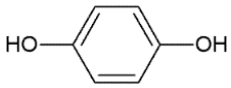		0.63 mol%	100 % (0.13 h)	0.0208	99.04
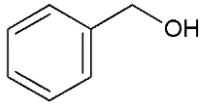	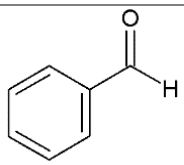	0.62 mol%	8 % (0.5 h)	0.0888	107.43
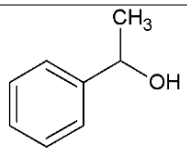	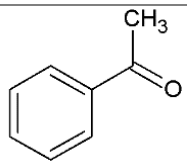	0.73 mol%	20 % (0.5 h)	0.0796	124.53
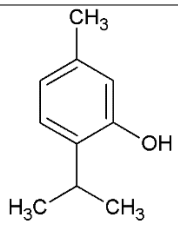	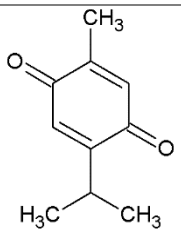	0.89 mol%	-	0.0989	158.45

[a] Relative concentrations of substrate and product were determined from UV-vis spectra of each reaction after the specified time. Calculation was not possible for TH due to overlapping product and reactant UV-vis spectra and lack of extinction coefficient for oxidised product. All reactions were carried out with 15 mg of substrate in 1 mL of AcN and initiated by addition of 50 µL of 70 % (w/w) ^{t}BuOOH in water at 25 °C. All reactions were followed by UV-vis spectroscopy ; [b] Half-lives were determined from UV-vis spectroscopy data obtained at 25.00 °C, fitted with a non-linear regression model in GraphPad Prism (Fig S24)[3]; [c] molecular volume was calculated using Chemicalize.[4]

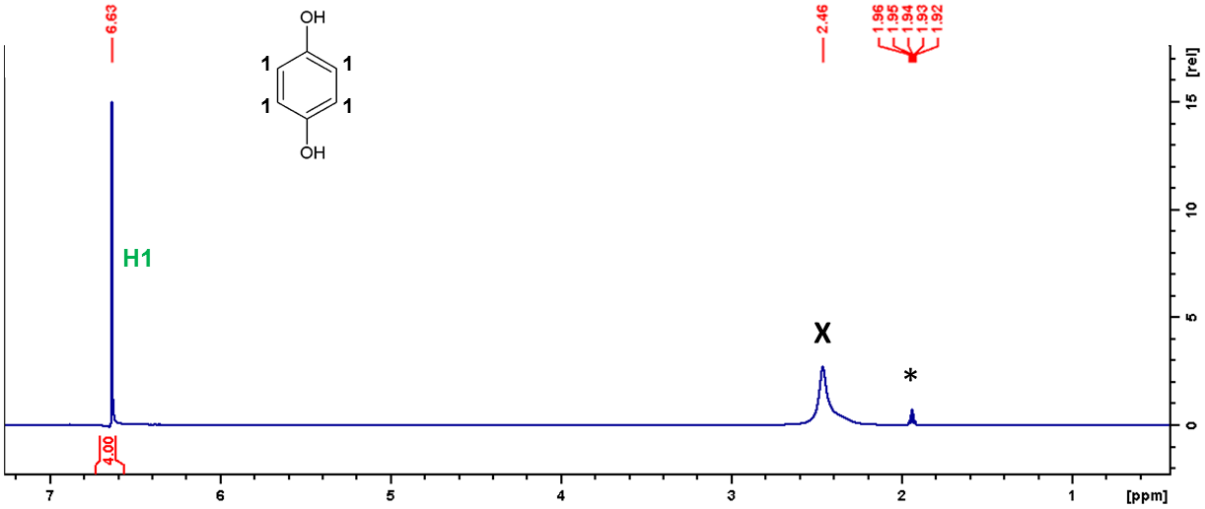

Figure S18: *^{1}H NMR spectrum of hydroquinone in acetonitrile-d_3. Asterisks (*) indicate the presence of residual AcN and (**X**) indicates peak due to H_2O. Labelled signal in green (δ 6.63) indicates signal from CH protons of hydroquinone used for monitoring of reaction and % conversion.*

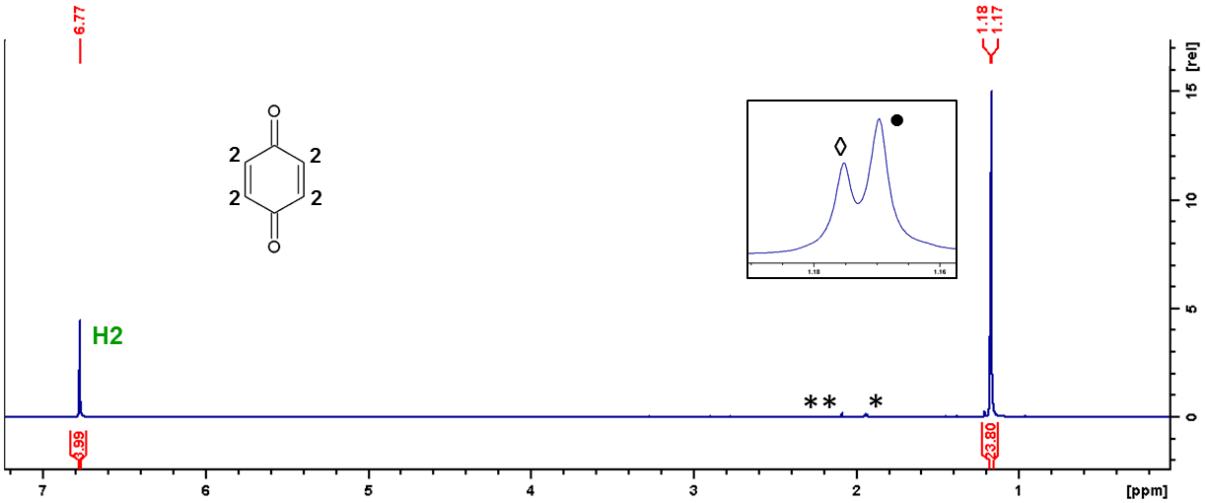

***Figure S19**: ^{1}H NMR spectrum of benzoquinone product in acetonitrile-d_3. Spectrum was recorded after in situ reaction of hydroquinone with [t]BuOOH after 24 hours and following filtration of Fe(III)PPIX-**1**. Pre-saturation pulse programme was used to minimize the peak due to water. Asterisks indicate the presence of residual AcN (*) and acetone (**); (●) indicates peak due to tBuOH and (◊) indicates peak due to [t]BuOOH. Labelled signal in green (δ 6.77) indicates signal from CH protons of benzoquinone used for monitoring of reaction and % conversion. No signal from CH protons of hydroquinone (δ 6.63) is observed.*

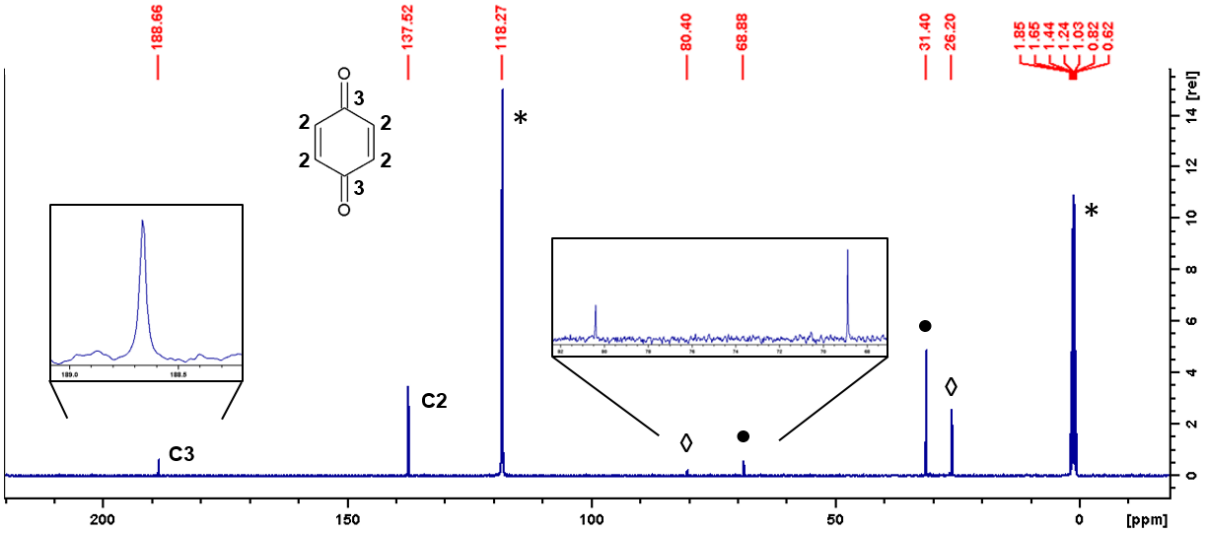

Figure S20: *^{13}C NMR spectrum of benzoquinone product in acetonitrile-d_3. Spectrum was recorded after in situ reaction of hydroquinone with ^{t}BuOOH after 24 hours and following filtration of Fe(III)PPIX-**1**. Asterisks indicate the presence of residual AcN (*); (●) indicates peak due to tBuOH and (◊) indicates peak due to tBuOOH.*

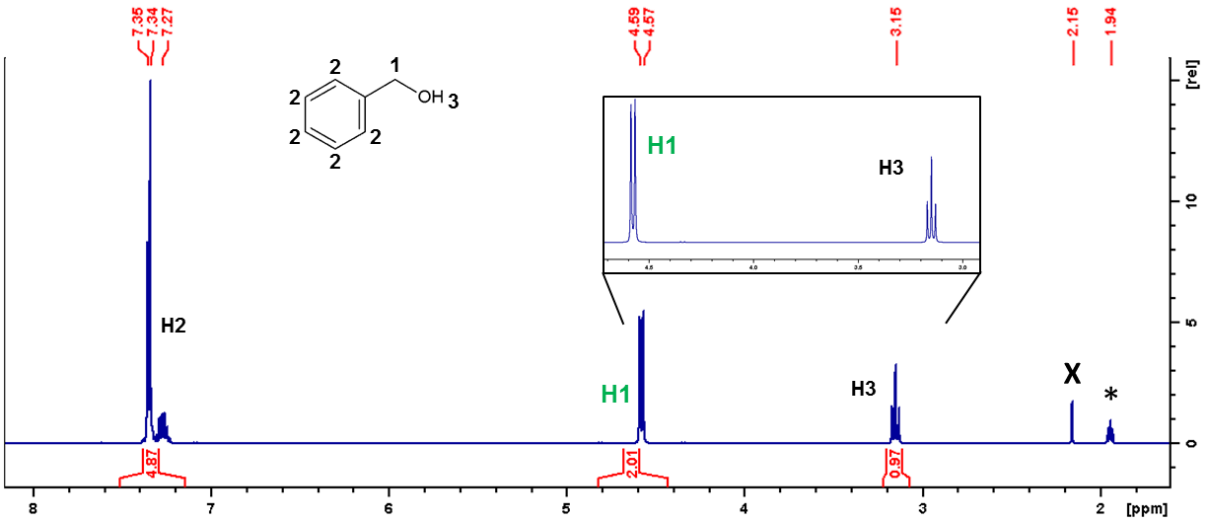

Figure S21: *^{1}H NMR spectrum of benzyl alcohol in acetonitrile-d_3. Asterisk (*) indicates residual AcN and (**X**) indicates water peak. Labelled signal in green (δ 4.57) indicates signal from CH_2 protons of benzyl alcohol used for monitoring of reaction and % conversion.*

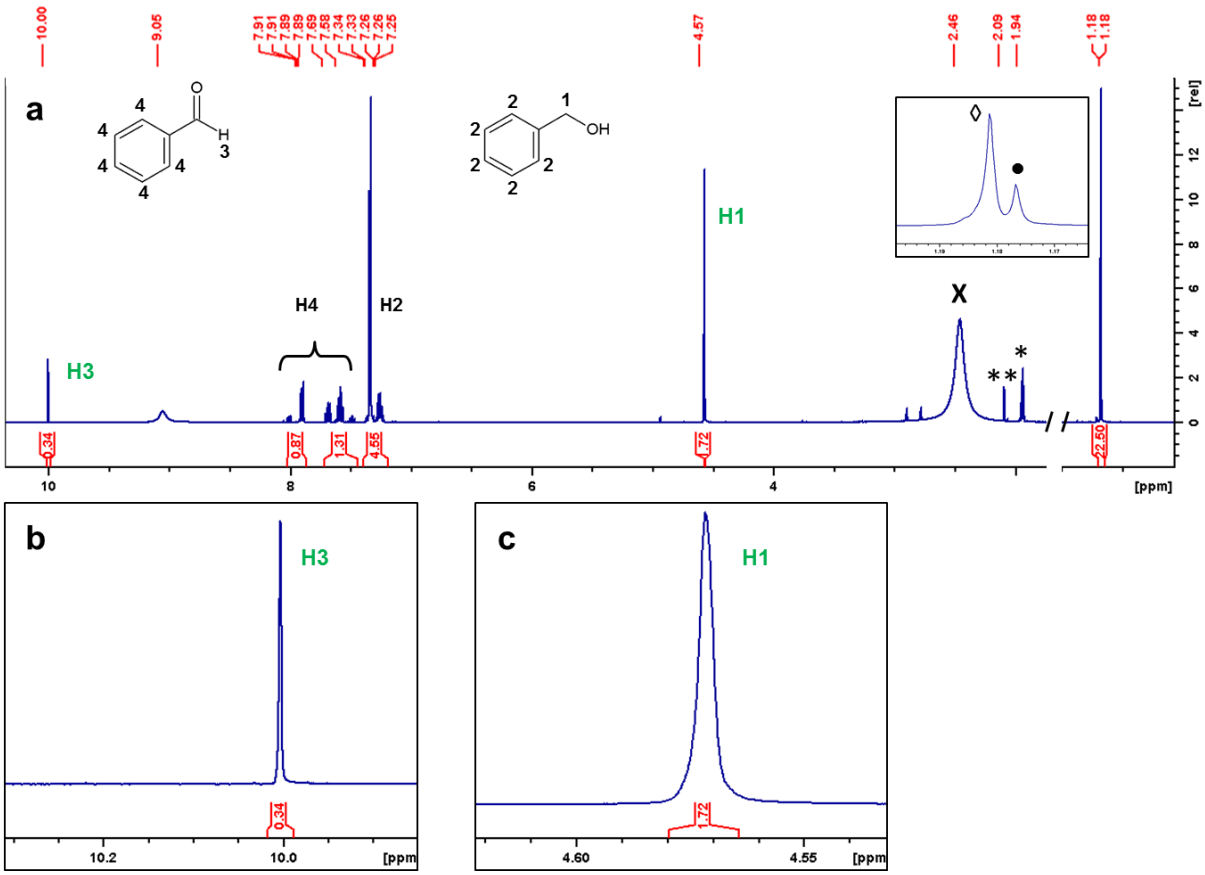

***Figure S22**: (a) ^{1}H NMR spectrum of benzaldehyde product and benzyl alcohol in acetonitrile-d_3. Spectrum was recorded after in situ reaction of hydroquinone with ^{t}BuOOH after 48 hours following filtration of Fe(III)PPIX-**1**. Asterisks indicate the presence of residual AcN (*) and acetone (**); (**X**) denotes a water peak and (●) indicates peak due to ^{t}BuOH and (◊) indicates peak due to ^{t}BuOOH. Labelled protons in green indicate integration used for monitoring of reaction and % conversion. (b) and (c) expansion of aldehyde proton (δ 10.00) from benzaldehyde (b) and CH_2 protons (δ 4.57) respectively used for conversion % calculation and to monitor the reaction progress.*

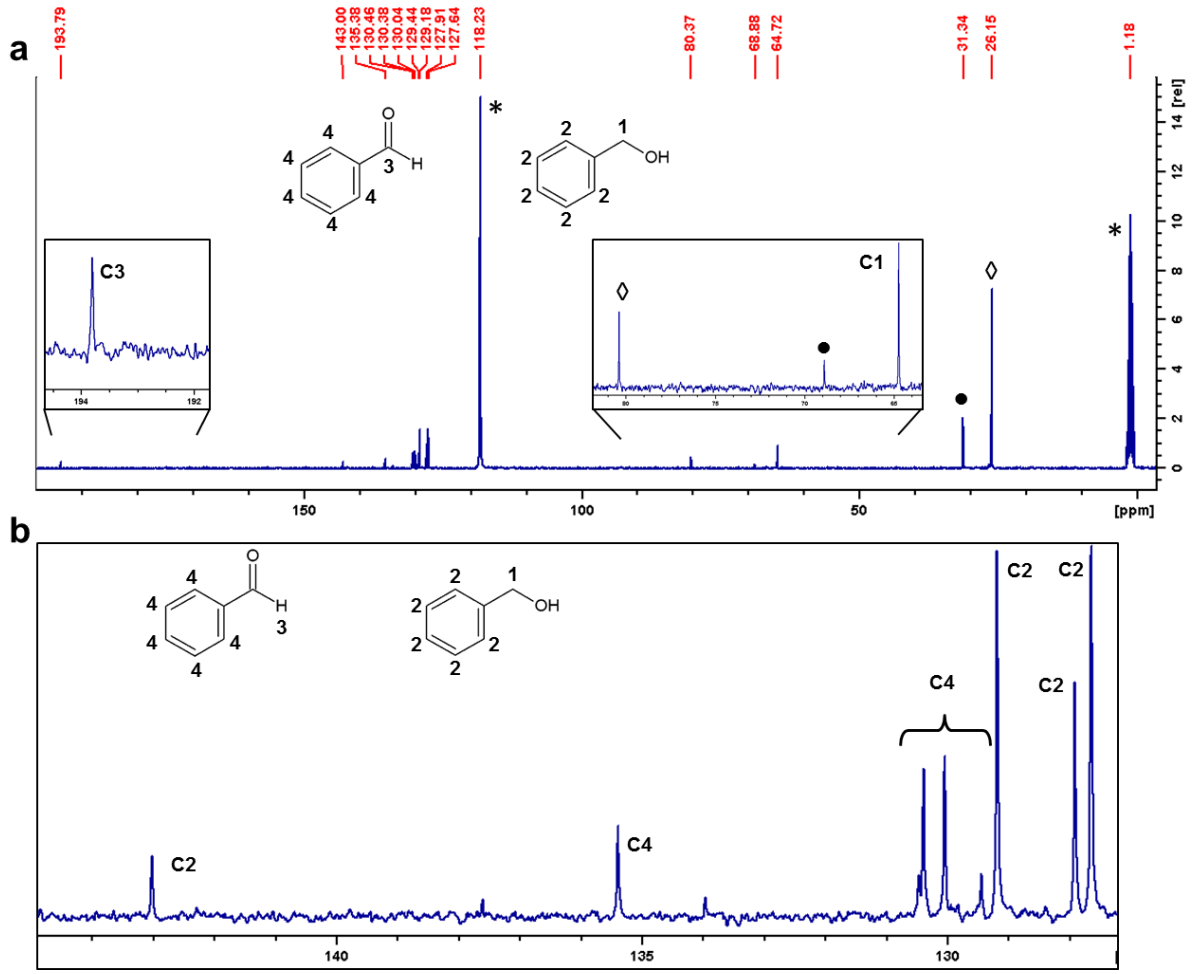

***Figure S23**: (a) ^{13}C NMR spectrum of benzyl alcohol and benzaldehyde product in acetonitrile-d_3. Spectrum was recorded after in situ reaction of hydroquinone with ^{t}BuOOH for 24 hours and following filtration of Fe(III)PPIX-**1**. Asterisks indicate the presence of residual AcN (*); (●) indicates peak due to ^{t}BuOH and (◊) indicates peak due to ^{t}BuOOH; (b) expansion of aromatic region of the same spectrum.*

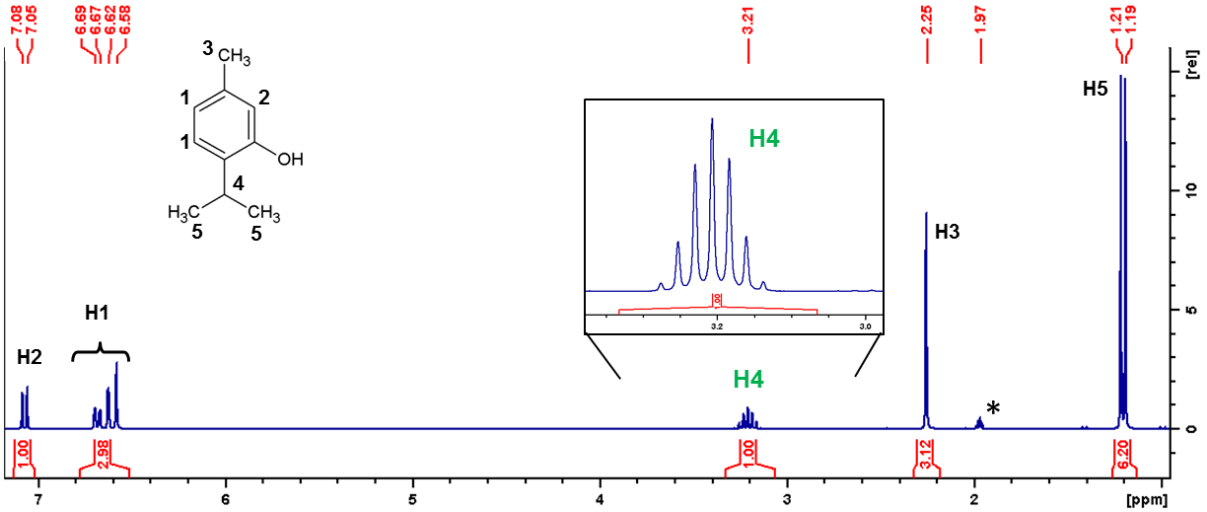

Figure S24: *^{1}H NMR spectrum of thymol in acetonitrile-d_3. Asterisk (*) indicates residual AcN. Labelled signal in green (δ 3.21) indicates signal from CH proton of thymol used for monitoring of reaction and % conversion.*

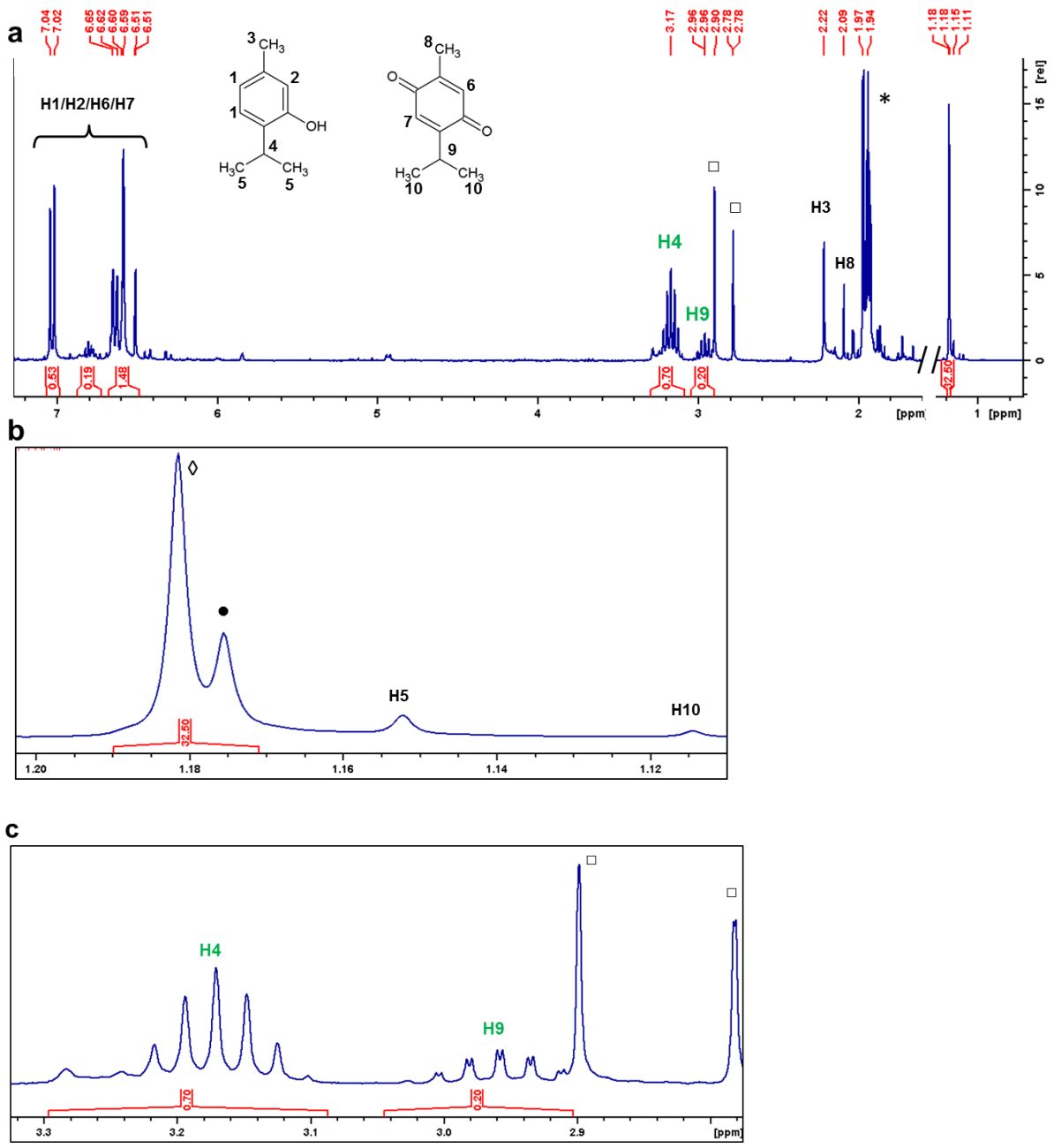

***Figure S25**: (a) ^{1}H NMR spectrum of thymol quinone product and thymol in acetonitrile-d_3. Spectrum was recorded after in situ reaction of hydroquinone with ^{t}BuOOH after 48 hours following filtration of Fe(III)PPIX-**1**. Presaturation pulse programme was used to minimize the peak due to water. Asterisk indicates the presence of residual AcN (*); (●) indicates peak due to ^{t}BuOH ; (◊) indicates peak due to ^{t}BuOOH and (□) indicates peaks due to DMF from the*

catalyst. Labelled protons in green indicate integration used for monitoring of reaction and % conversion. (b) Expansion of region where isopropyl protons from thymol (H5) and thymoquinone (H10) are observed. (c) Expansion of signal from CH proton of thymol (δ 3.17) and thymoquinone (δ 2.96) respectively used for conversion calculation and reaction monitoring. Conversion of thymol to thymoquinone was too low to see the quinone product using ^{13}*C NMR.*

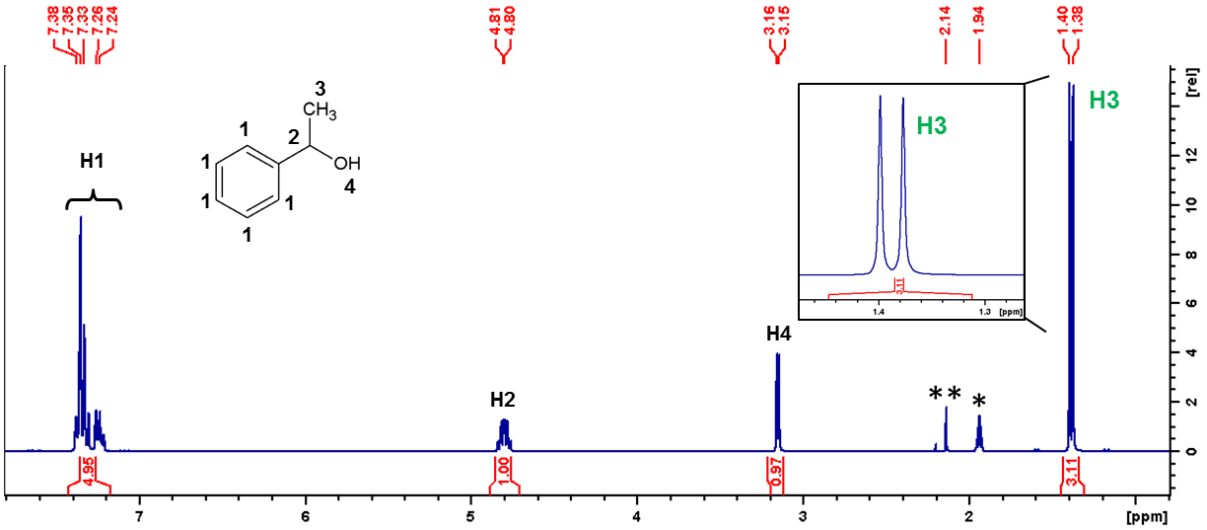

Figure S26*: ^{1}H NMR spectrum of phenyl ethanol in acetonitrile-d$_3$. Asterisks (*) indicates residual AcN and (**) acetone. Labelled signal in green (δ 1.38) indicates signal from CH$_3$ proton of phenyl ethanol used for monitoring of reaction and % conversion.*

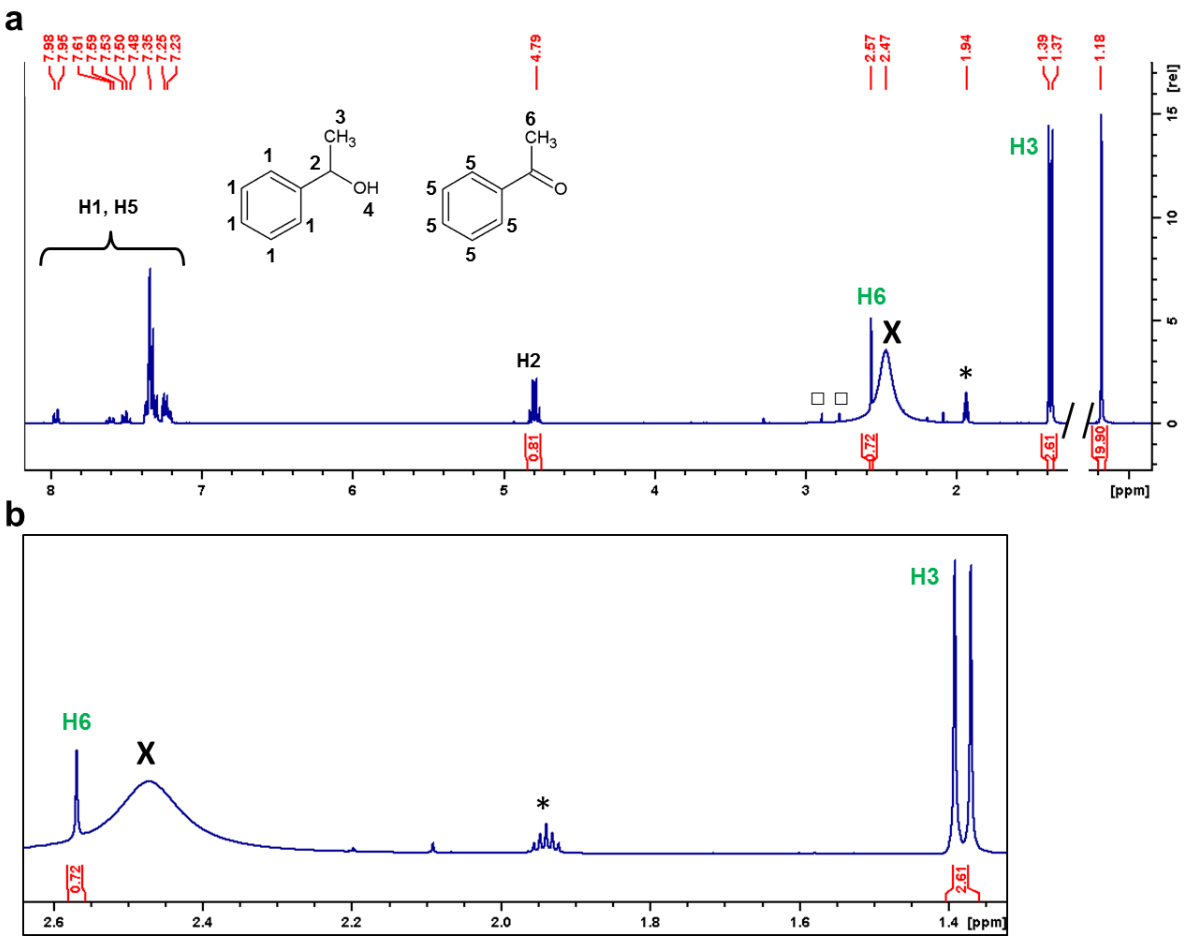

Figure S27: *(a) ^{1}H NMR spectrum of acetophenone product and phenyl ethanol in acetonitrile-d_3. Spectrum was recorded after in situ reaction of hydroquinone with ^{t}BuOOH after 48 hours following filtration of Fe(III)PPIX-**1**. Asterisk indicates the presence of residual AcN (*) and acetone (**X**); (□) indicates peaks due to DMF from the catalyst. Labelled protons in green indicate integration used for monitoring of reaction and % conversion. (b) Expansion of signal from CH_3 protons from phenyl ethanol (δ 1.39) and acetophenone (δ 2.57) respectively used for conversion calculation and reaction monitoring. Conversion of phenyl ethanol to acetophenone was too low to see the acetophenone product using ^{13}C NMR.*

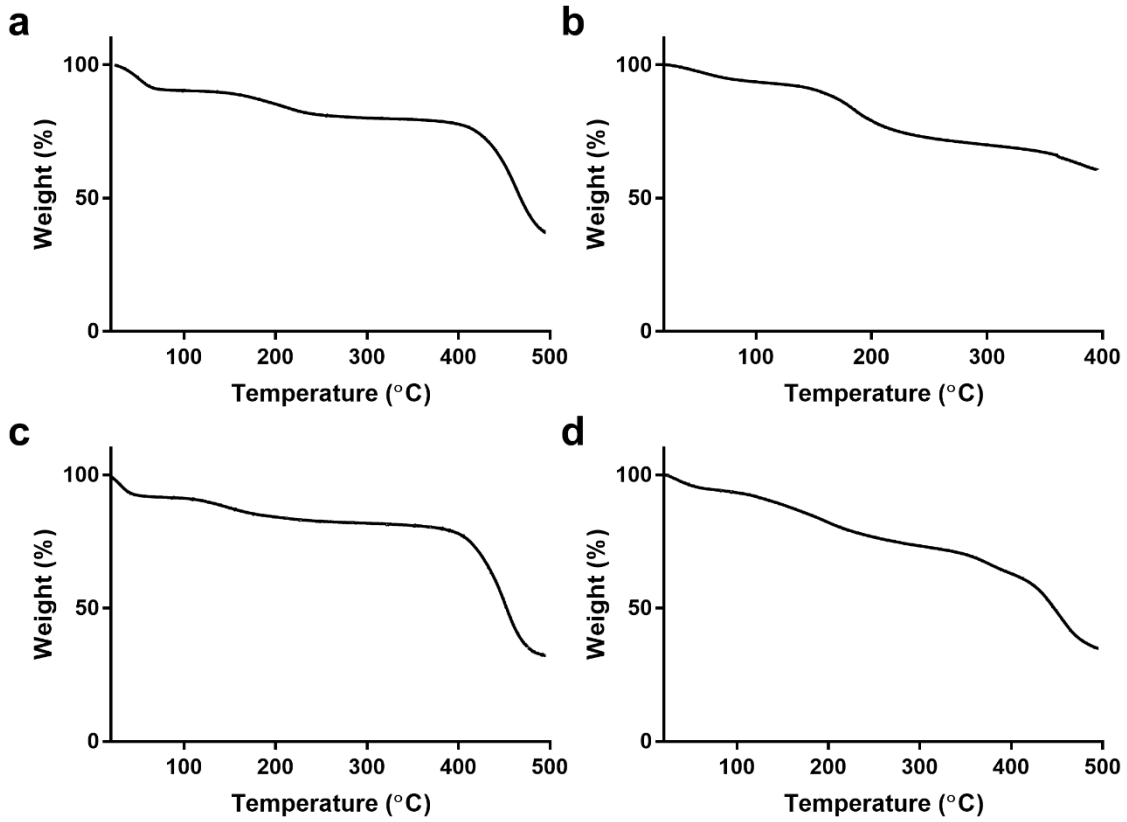

Figure S28*: TGA of (a)* ***1****, (b)* ***2****, (c) Fe(III)PPIX-****1*** *and (d) Fe(III)PPIX-****2****.*

*Table S2: Crystallographic data for the single crystal X-ray structure of **1** and Fe(III)PPIX-**1***

	1	Fe(III)PPIX-**1**
Chemical Formula	$Zn_3C_{56}N_9O_{21}H_{59}$	$Zn_3C_{54.12}N_{6.72}O_{13.72}Fe_{0.18}$
Molar mass (g mol^{-1})	1390.23	1119.89
Crystal System	Tetragonal	Tetragonal
Space Group	$P4_322$	$P4_1$
a (Å)	17.9300(9)	18.0063(4)
c (Å)	26.0524(13)	26.5714(10)
V (Å^3)	8375.5(9)	8615.2(4)
Z	4	4
$\rho_{calcd.}$ (g cm^{-3})	0.886	0.852
μ (mm^{-1})	0.895	0.831
λ (Å)	0.71073	0.6889(3)
F(000)	2248	2221
Temperature (K)	173(2)	100(2)
Crystal size (mm)	0.38 × 0.14 × 0.13	0.64 × 0.52 × 0.512
Range scanned θ (°)	1.379 – 28.429	1.719 – 24.919
Total number of reflections	153876	50940
Number of independent reflections	10487	50940
Number of reflections with $I > 2\sigma(I)$	8899	38880
R_{int}	0.0604	0.1286
$R_1(F)$ [a] [$I > 2\sigma$(I)]	0.0552	0.1495
$wR_2(F^2)$ [a]	0.1968	0.3255
$S(F^2)$ [a]	1.162	1.187
Number of parameters (p)	323	653
Number of restraints (r)	2	10
Number of reflections omitted	2	55
$(\delta/\sigma)_{mean}$	<0.001	<0.001
Max./min Δρ excursions (e Å^{-3})	-0.602; 1.909	-0.807; 1.935

[a] $R1(F) = \Sigma(|F_o| - |F_c|)/\Sigma|F_o|$; $wR_2(F^2) = [\Sigma w(F_o^2 - F_c^2)^2/\Sigma wF_o^4]^{½}$; $S(F^2) = [\Sigma w(F_o^2 - F_c^2)^2/(n + r - p)]^{½}$

References:

(1) Sun, D.; Ke, Y.; Collins, D. J.; Lorigan, G. A.; Zhou, H.-C. Construction of Robust Open Metal−Organic Frameworks with Chiral Channels and Permanent Porosity. *Inorg. Chem.* **2007**, *46*, 2725–2734.

(2) Feldblyum, J. I.; Liu, M.; Gidley, D. W.; Matzger, A. J. Reconciling the Discrepancies between Crystallographic Porosity and Guest Access As Exemplified by Zn-HKUST-1. *J. Am. Chem. Soc.* **2011**, *133*, 18257–18263.

(3) *GraphPad Prism v6.05*; GraphPad Software: San Diego, CA, 2014.

(4) ChemAxon. *Chemicalize*; 2017.